CCS Chemistry

RESEARCH ARTICLE

Received: Nov. 30, 2020 | Accepted: Jan. 3, 2021

A Multiresponsive Transformation between Surfactant-Based Coacervates and Vesicles

Lili Zhou[1,2], Yaxun Fan[1]*, Zhang Liu[1], Lina Chen[3], Evan Spruijt[3]* & Yilin Wang[1,2]*

[1]*CAS Key Laboratory of Colloid, Interface and Chemical Thermodynamics, CAS Research/Education Center for Excellence in Molecular Sciences, Beijing National Laboratory for Molecular Science, Institute of Chemistry, Chinese Academy of Sciences, Beijing 100190,* [2]*University of Chinese Academy of Sciences, Beijing 100049,* [3]*Institute for Molecules and Materials, Radboud University, 6525 AJ Nijmegen*

**Corresponding authors: yxfan@iccas.ac.cn; e.spruijt@science.ru.nl; yilinwang@iccas.ac.cn*

Cite this: *CCS Chem.* **2021**, *3*, 358–366

Low-molecular weight surfactants have significant potential as building blocks for prebiotic organization. However, reports about surfactant-based coacervates as protocell models capable of reversible transformation are scarce. Herein, we develop a simple system made of a surfactant (–)-*N*-dodecyl-*N*-methylephedrinium bromide (DMEB) and inorganic salts that is capable of spontaneous formation of vesicles, coacervates, and the reversible transformation between the two states. The coacervates are stable over a wide range of pH values and salt concentrations, and they contain a disordered sponge-like internal microstructure, which leads to effective encapsulation of a broad range of solutes and biomacromolecules such as DNA and green fluorescent protein (GFP). They provide an advantageous chemical environment in which the activity of enzymes, including apyrase, is enhanced. Strikingly, these coacervates can undergo a reversible transformation to small, well-defined vesicles by changing the temperature and surfactant or salt concentrations. Moreover, we show that this transition can be dynamically controlled by chemical reactions. The cycling between open (coacervates) and closed (vesicles) compartments could facilitate the encapsulation of solutes within membrane-bound vesicles, and our results demonstrate that these surfactant-based coacervates constitute superior protocells capable of a reversible droplet-vesicle transition.

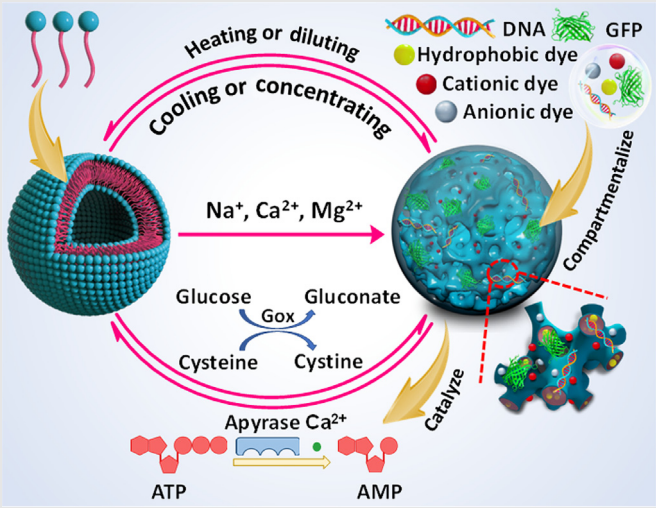

Keywords: coacervates, sequestration, microreactors, reversible transformation, vesicles

Introduction

Coacervates have increasingly been recognized as one of three main categories of protocell models or synthetic cells besides vesicular structures and their combinations.[1–10] Such liquid-like microdroplets provide a promising means to spontaneously sequester a wide range of chemical and biological components,[11–13] thereby

DOI: 10.31635/ccschem.021.202000702
CCS Chem. **2021**, *3*, 358–366

producing aspects of the crowded interiors of cells and speeding up relevant protometabolic and biochemical reactions.[14–18] Their membrane-free nature also favors unhindered exchange of matter with their surroundings.[19,20] Therefore, the design of dynamic coacervate-based systems is a vibrant research area in the synthetic cell community.

Coacervate-based protocell models can be produced from biological or nonbiological components, but most of them are assembled spontaneously from aqueous mixtures of high-molecular weight polymers, such as biological macromolecules, multivalent proteins, polysaccharides, and neutral or synthetic polyelectrolytes.[12,14,18] Recently reported hybrid models are based on coacervates constructed by polyelectrolytes of high concentration but covered by fatty acid or lipid membranes.[7,9] However, high-molecular weight components are presumably not present in a prebiotic milieu.[7,19] By contrast, less complex and potentially abundant lower-molecular weight surfactants with different headgroups and hydrophobic chains have been proposed as possible constituents of early membranes.[21–24] Thus, they could be the potential building blocks for prebiotic organization, but more effort is required to create coacervates from single-chain surfactants and develop various bioinspired functions including enhancing bioreaction rate in such systems, which has only been found in polymer-based coacervates.[25–29]

Although the lack of membranes endows coacervates with the ability to act as open compartments and favors exchange of matter with the environment, it also makes coacervates potentially unstable in the long term, due to the partitioning of passive solutes, spontaneous droplet fusion, and so forth. Systems capable of reversible transition between coacervates and a different organizational state (solution, micelles, and vesicles) upon changes in temperature, pH, concentration, and so forth provide a promising strategy for dynamically controlling material exchange and conferring on protocells the ability to sustain metabolic reactions.[30–36] The ability to switch from membrane-free coacervates to membrane-bound vesicles is an especially attractive way to combine the advantages of efficient sequestration in coacervates with long-term stability of compartments and a direct link to the appearance of modern cell membranes. So far, only one reversible coacervate-to-vesicle transition, together with spontaneous protein encapsulation, has been realized in a myristic acid/guanidine hydrochloride system by adjusting pH.[25] The dynamic control in this system is, however, limited. As a matter of fact, coacervates as protocell models could dynamically respond to different environmental cues, such as concentration, temperature, and even chemical reactions.

Herein, we develop a superior surfactant-based coacervate system, as a membrane-free protocell model, that can undergo a reversible transition to small, well-defined vesicles in response to a wide variety of triggers. The coacervates are based on the spontaneous phase separation of a single-chain surfactant (−)-*N*-dodecyl-*N*-methylephedrinium bromide (DMEB; Figure 1a) in the presence of NaCl, $CaCl_2$, or $MgCl_2$. They are readily formed at low DMEB concentrations and remain stable over a broad range of pH values and as the salt concentration reaches the limit of solubility. A wide range of dyes and biomacromolecules, including enzymes, are spontaneously taken up and remain active inside the coacervates, assisting to enhance the reaction rate. Importantly, DMEB can also form vesicles, and we use this property to establish a reversible transition between coacervates and vesicles. The transition can be effectuated by changes in temperature, concentration, salt concentration, and small biological metabolites. We can use chemical reactions to control the formation of these metabolites and realize an active system of morphology-changing compartments from coacervates to vesicles and back.

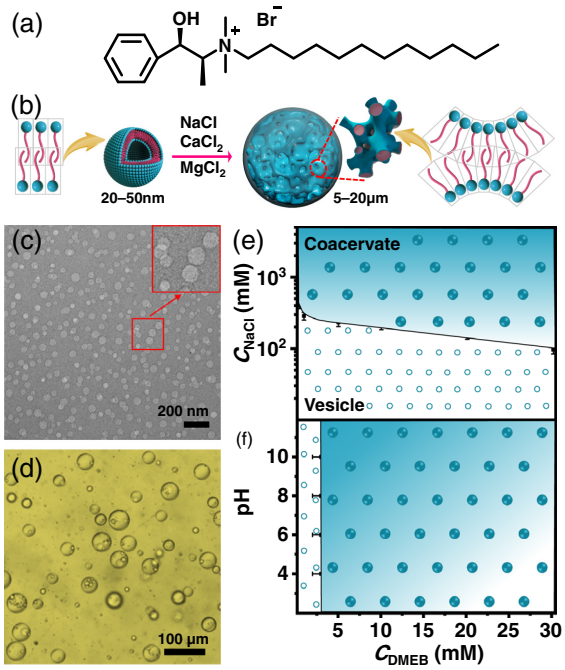

Figure 1 | *Coacervation in the mixture of DMEB with inorganic salts. (a) Chemical structure of DMEB. (b) Schematic representation of phase transitions after adding salts (NaCl, $CaCl_2$, and $MgCl_2$) to DMEB, and schematic illustrations of the proposed molecular packing and internal microstructures of vesicles and coacervates. (c) Cryo-TEM image of vesicles in 30 mM DMEB/75 mM NaCl mixed solution. (d) Bright-field microscopy image of coacervate droplets in 10 mM DMEB/250 mM NaCl mixed solution. (e) Phase diagram of DMEB/NaCl mixtures at pH 7. The coacervates exist until the saturation solubility of NaCl (~5 M). (f) Phase diagram of DMEB with 250 mM NaCl at different pH values (2–12). Blue and colorless areas represent coacervate and vesicle region, respectively.*

DOI: 10.31635/ccschem.021.202000702
CCS Chem. **2021**, *3*, 358–366

Experimental Methods

Materials

DMEB, α-D-glucose, and glucose oxidase (Gox) from *Aspergillus niger* (100 KU), L-cysteine, adenosine 5′-triphosphate (ATP) disodium, and apyrase from potato (100 UN) were purchased from Sigma-Aldrich (Beijing, China). NaCl, $MgCl_2$, $CaCl_2$, rhodamine 6G, fluorescein, and calcein were obtained from J&K (Beijing, China). Methylene blue was purchased from Alfa (Beijing, China). Nile red was purchased from Acros (Beijing, China). Alex488-labeled DNA was purchased from Integrated DNA Technologies (IDT; Leuven, Belgium). Green fluorescent protein (GFP) was obtained from Thermo Fisher Scientific (Beijing, China). All the reactants were used without further purification. All the solutions were prepared in Milli-Q water (18 MΩ·cm^{-1}).

Characterizations

The turbidity was measured using a Brinkman PC920 (Brinkmann, Westbury, USA) probe colorimeter thermostat. Dynamic light scattering (DLS) was performed by a Zetasizer Nano ZS (Malvern, Malvern, UK) equipped with a 4 mW He–Ne laser (λ = 633 nm). Cryogenic transmission electron microscopy (cryo-TEM) was imaged with a JEM-2010 TEM (JEOL, Tokyo, Japan). The morphology of the coacervate droplets was characterized by cryogenic scanning electron microscopy (cryo-SEM) using a HITACHI S-4300 SEM (Hitachi, Tokyo, Japan). Optical microscopy images of the phase separation were captured by an optical microscope [XSP-8C(8CA) (Teelen, Shanghai, China)] with a mounted digital camera. Fluorescence microscopy images were recorded on an Olympus IX83 microscope (Olympus, Tokyo, Japan). Confocal microscopy imaging was performed using a Leica SP5-II laser scanning microscope attached to a Leica DMI6000 (Leica, Mannheim, Germany). NMR measurements were recorded on a Bruker AV400 FT-NMR spectrometer (Bruker, Billerica, USA).

Other characterization methods and experimental details (including preparation of coacervate droplets, phase diagram, sequestration of hydrophilic/hydrophobic dyes and biomacromolecules in coacervates, partition coefficients of dye and biomacromolecule in coacervates, enhancement of bioreaction rate within coacervates, and multiresponsive phase transitions) are available in the Supporting Information.

Results and Discussion

Coacervation in the mixture of DMEB with inorganic salt

The transition from vesicles to coacervates of DMEB aqueous solutions was investigated by turbidity titrations, cryo-TEM, and light microscopy. DMEB had low solubility at room temperature, but when dissolved in H_2O, formed vesicles when the concentration was above its critical micelle concentration (4 mM) and below 50 mM at 30 °C.[37,38] By increasing the concentration of DMEB, the size (Supporting Information Figure S1a) sharply increased from 20–50 nm of vesicle (Supporting Information Figure S1b) to 5–20 μm of coacervate (Supporting Information Figure S1c) at 50 mM DMEB, which corresponded to the vesicle-to-coacervate transition. When monovalent salt was added (C_{NaCl} > 100 mM), either vesicles or coacervates stably existed at 25 °C by mixing the transparent DMEB and NaCl stock solutions. The DMEB concentration at which this transition occurred decreased by two orders of magnitude at pH 7, down to 0.5 mM (Figure 1b), which was evidenced by the transformation of 30–40 nm vesicles (Figure 1c and Supporting Information Figure S2) into turbid dispersions of 20–70 μm-sized spherical droplets (Figure 1d and Supporting Information Figures S3a–S3c). The fusion and enlargement of the coacervate droplets confirmed their liquid, membrane-free state (Supporting Information Figure S4 and Movie S1). The droplets were larger than observed in salt-free DMEB solutions and in general polymer-based coacervates, and the condensed coacervate phase was transparent and nonbirefringent. Furthermore, the coacervate droplets were stable over a wide range of DMEB concentration, NaCl concentration, and pH values as depicted in phase diagrams (Figures 1e and 1f) derived from the turbidity curves of the DMEB/NaCl aqueous solution as a function of NaCl concentration at pH 7 (Supporting Information Figure S5a) or as a function of pH at 250 mM NaCl (Supporting Information Figure S6a). The suspensions were diluted up to 10-fold (e.g., 30 mM DMEB/3 M NaCl) without destabilizing the droplets. Notably, a small but perceptible dependence on pH is shown in the turbidity curve for 5 mM DMEB/250 mM NaCl. Under alkali conditions, the Br^- was replaced by OH^- inducing better DMEB solubility and a larger headgroup area because the associated OH^- ion had stronger affinity for water and stayed further from the charged surface than Br^-.

Generally, multivalent cationic metal ions such as Ca^{2+} and Mg^{2+} can significantly decrease the solubility of a surfactant in water.[39] As a consequence, coacervation of DMEB was enhanced by divalent salts ($CaCl_2$ and $MgCl_2$; Supporting Information Figures S3d and S3e), and the coacervates remained stable until the solubility limit of both salts (Supporting Information Figures S5b, S5c, S7a, and S7c), at pH 2–12 for $CaCl_2$ (Supporting Information Figures S6b and S7b), or 2–10 for $MgCl_2$ (Supporting Information Figures S6c and S7d). Since many bioreactions require Ca^{2+}[40,41] and Mg^{2+}[42,43] as catalyst, we hypothesize that the enhanced DMEB coacervate formation by NaCl, $CaCl_2$, and $MgCl_2$ could be the basis for a new type of protocell model with catalytic functions, and their

DOI: 10.31635/ccschem.021.202000702
CCS Chem. **2021**, *3*, 358–366

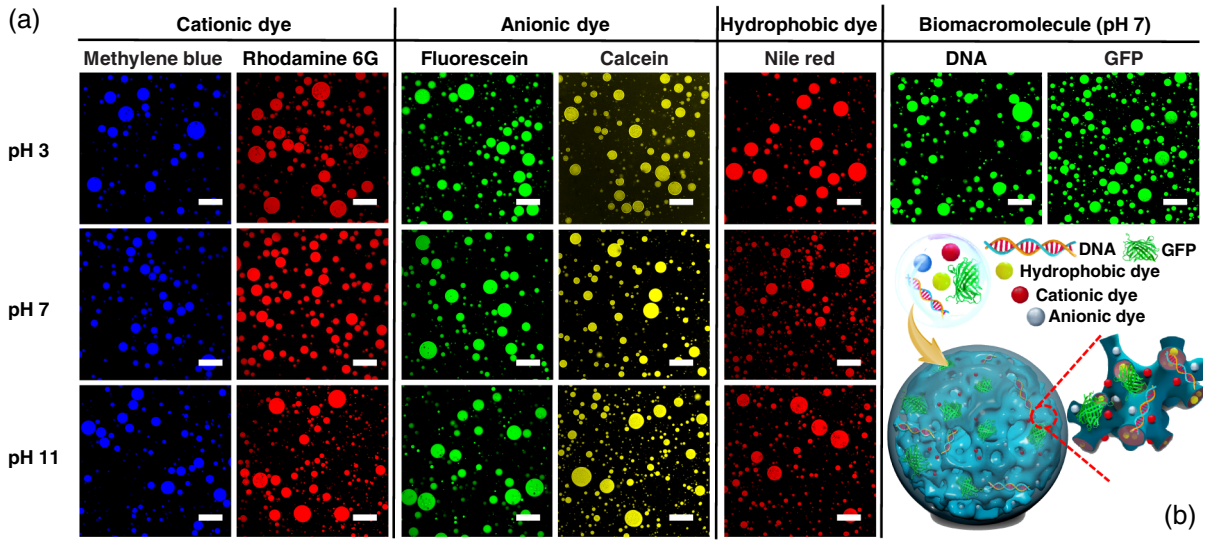

Figure 2 | *Sequestration of hydrophilic/hydrophobic dyes and biomacromolecules in DMEB/NaCl coacervates. (a) Confocal fluorescence images of 0.05 mM cationic dyes (methylene blue and rhodamine 6G), anionic dyes (calcein and fluorescein), and hydrophobic dye (nile red) at pH 3, 7, and 11, and biomacromolecules (5 μM Alex488-labeled dsDNA and 0.1 mg/mL GFP) at pH 7 in 10 mM DMEB/250 mM NaCl coacervates. The dyes and biomacromolecules all preferentially partition into the coacervates. Scale bar = 100 μm for all images. (b) Schematic illustration of sequestration of dyes and biomacromolecules in coacervate droplets.*

stability in a large pH range facilitates various bioreactions requiring different pH conditions.

It is widely believed that surfactant-based coacervates have a sponge-like bicontinuous structure, and their formation requires the negative Gaussian curvature (H_0) of bilayers.[44,45] This structure is made of randomly connected bilayer networks, locally resembling the topology of a bicontinuous cubic phase with short-range order. With addition of salts, the electrostatic repulsion between the charged headgroups of DMEB can be effectively screened, and the hydrophobic part becomes bulkier compared with its hydrophilic headgroup, thereby inducing the transition to coacervates with internal sponge-like microstructure (Figure 1b). Indeed, cryo-SEM images of the coacervates confirmed this sponge-like microstructure (Supporting Information Figure S3a). We hypothesized that the bicontinuous nature of the coacervates simultaneously facilitated the uptake and concentration of both hydrophobic and hydrophilic guest molecules.

Sequestration of hydrophilic/hydrophobic dyes and biomacromolecules in DMEB/salt coacervates

As a proof of concept, we tested if coacervates could encapsulate freely dissolved small molecules from the outside liquid phase without the need of dedicated transporters and localize high concentrations of macromolecules from a dilute external phase without a physical barrier, in which case both the small molecules and biomacromolecules of high concentrations can be compartmentalized. Indeed, cationic dyes (methylene blue and rhodamine 6G), anionic dyes (calcein and fluorescein), and hydrophobic dye (nile red) preferentially partitioned into the coacervates of DMEB/NaCl (Figures 2a and 2b), DMEB/$CaCl_2$ (Supporting Information Figure S8), and DMEB/$MgCl_2$ (Supporting Information Figure S9) at different pH values (pH <11 for DMEB/$MgCl_2$ because of solubility limit). Moreover, Alex488-labeled dsDNA (M_w = 15 kDa) and GFP (M_w = 27 kDa) were also trapped in the coacervates at pH 7. The partition coefficients (K) of the dyes[46,47] were quantified by UV–vis absorption spectroscopy in the two phases and summarized in Supporting Information Figure S10. The results indicated that the negatively charged and hydrophobic dyes were the most strongly sequestered (K > 200) into the coacervates, whereas positively charged dyes showed weaker, but still significant, partitioning (K close to 100). Meanwhile, the partition coefficients of DNA and GFP were estimated by the ratios of the fluorescence intensities inside and out of the droplets. The K values were all larger than 1000, also suggesting that the biomacromolecules were mainly sequestrated into the coacervates regardless of molecular weight. The efficient and broad-spectrum sequestration of solutes stands in sharp contrast to similar studies using single-component coacervates composed of fatty acids that showed no uptake of negatively charged dyes.[25,48] Improved sequestration could be attributed to the screening of surfactant

DOI: 10.31635/ccschem.021.202000702
CCS Chem. **2021**, *3*, 358–366

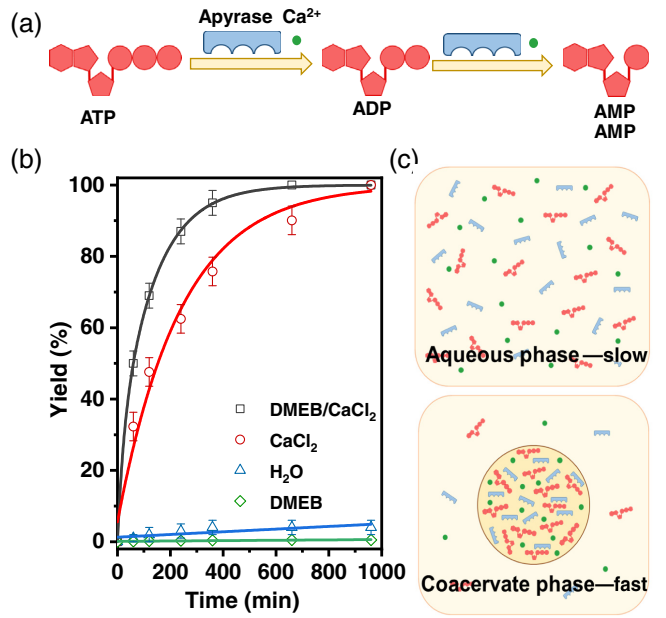

Figure 3 | *Kinetics for ATP hydrolysis in different phases. (a) Schematic representation of the process of ATP hydrolysis to AMP through a stepwise dephosphorylation with ADP as an intermediate, and calcium ion as a potent activator of potato apyrase. (b) Yield of AMP from the hydrolysis of 5 mM ATP as a function of time in pure water, 10 mM DMEB solution, 125 mM $CaCl_2$ solution, and 10 mM DMEB/125 mM $CaCl_2$ coacervates. (c) Schematic illustration of the effect of compartmentalization. The hydrolysis rate is enhanced by coacervates with compartmentalization of the enzyme, ATP, and Ca^{2+}, that is, an approximately 14-fold difference in effective rate between $CaCl_2$ solution and coacervate droplet.*

charges by inorganic salt ions and the disordered sponge-like internal microstructure of droplets with both hydrophilic and hydrophobic domains.

Kinetics for ATP hydrolysis in different phases

Because the compartmentalization increases the local concentrations of both small molecules and biomacromolecules, the coacervates could serve as a favorable medium for enzymatic reactions that otherwise would not occur or be limited in water.[49,50] As an example, we investigated the stepwise dephosphorylation of ATP via ADP to AMP by the enzyme apyrase, which requires calcium. Calcium-induced DMEB coacervates could sequester both the enzyme and substrates and provide an ideal environment for this reaction. We measured the rate of ATP hydrolysis in 10 mM DMEB/125 mM $CaCl_2$ coacervates and compared it with the rates in pure water, 10 mM DMEB vesicular solution, and 125 mM $CaCl_2$ aqueous solution (Figure 3a). Kinetics of this enzymatic reaction monitored by ^{31}P NMR showed a gradual increase in the yield of AMP versus time (Figure 3b and Supporting Information Figure S11). Without Ca^{2+}, the ATP hydrolysis was almost halted in pure water and 10 mM DMEB vesicular solution because Ca^{2+} is required to produce the active metal ion-nucleotide complex with the ATP substrate.[40,41] As expected, the hydrolysis rate was markedly enhanced with the addition of 125 mM Ca^{2+} in water. Interestingly, the rates were even further enhanced in 10 mM DMEB/125 mM $CaCl_2$ coacervates. The hydrolysis in solution in the presence and absence of calcium was fitted with a single exponential, and the fold change between them k_{rel} (k_{Ca}/k_{H2O}) was 1300 ± 400. In the case of coacervates, the hydrolysis data were fitted with a double exponential equation, corresponding to the reaction taking place inside and outside of the coacervates. The fold change of the two rate constants with respect to the vesicular solution without calcium was 18,000 ± 9000 and 2100 ± 600, respectively (Supporting Information Table S1). In the presence of coacervate, the ATP concentration was enriched to 320 mM in the coacervate phase, about 60-fold higher than that of the initial concentration (5 mM; Supporting Information Figure S12). The approximately 14-fold difference in effective rate between $CaCl_2$ solution and coacervate droplet could be attributed to the increased local concentration of substrate and enzyme due to compartmentalization inside the coacervates (Figure 3c). On the other hand, the weakly charged ADP and AMP may be more easily released from the DMEB coacervates than ATP, which would facilitate the separation of ADP or AMP from ATP and enhance the reaction rate along with the comparable production yields. In addition to the biocatalysis of these inorganic ions in many other bioreactions,[51,52] the DMEB/$CaCl_2$ and DMEB/$MgCl_2$ coacervates have the potential to accelerate the bioreaction rates as metabolic protocell models endowing sequestration ability and catalytic activity simultaneously.

Phase transitions between vesicles and coacervates

Coacervates as protocell models are inherently dynamic and can form or disassemble in response to environmental cues, when and where needed. The systems capable of reversible transition between membrane-free (coacervates) to membrane-bound one (vesicles) provide an alternative strategy for dynamically controlling the exchange of matter and long-term solute segregation in a closed compartment.[25,34] To prove that this type of phase transition can be controlled in a reversible way using various mechanisms in our surfactant-based system, we designed a reversible cycle between coacervates and vesicles triggered by temperature, concentration, and chemical reactions (Figure 4a).

The turbidity titration curves corresponding to heating and cooling processes are almost symmetric without obvious hysteresis, displaying that the DMEB/salt system

DOI: 10.31635/ccschem.021.202000702
CCS Chem. **2021**, *3*, 358–366

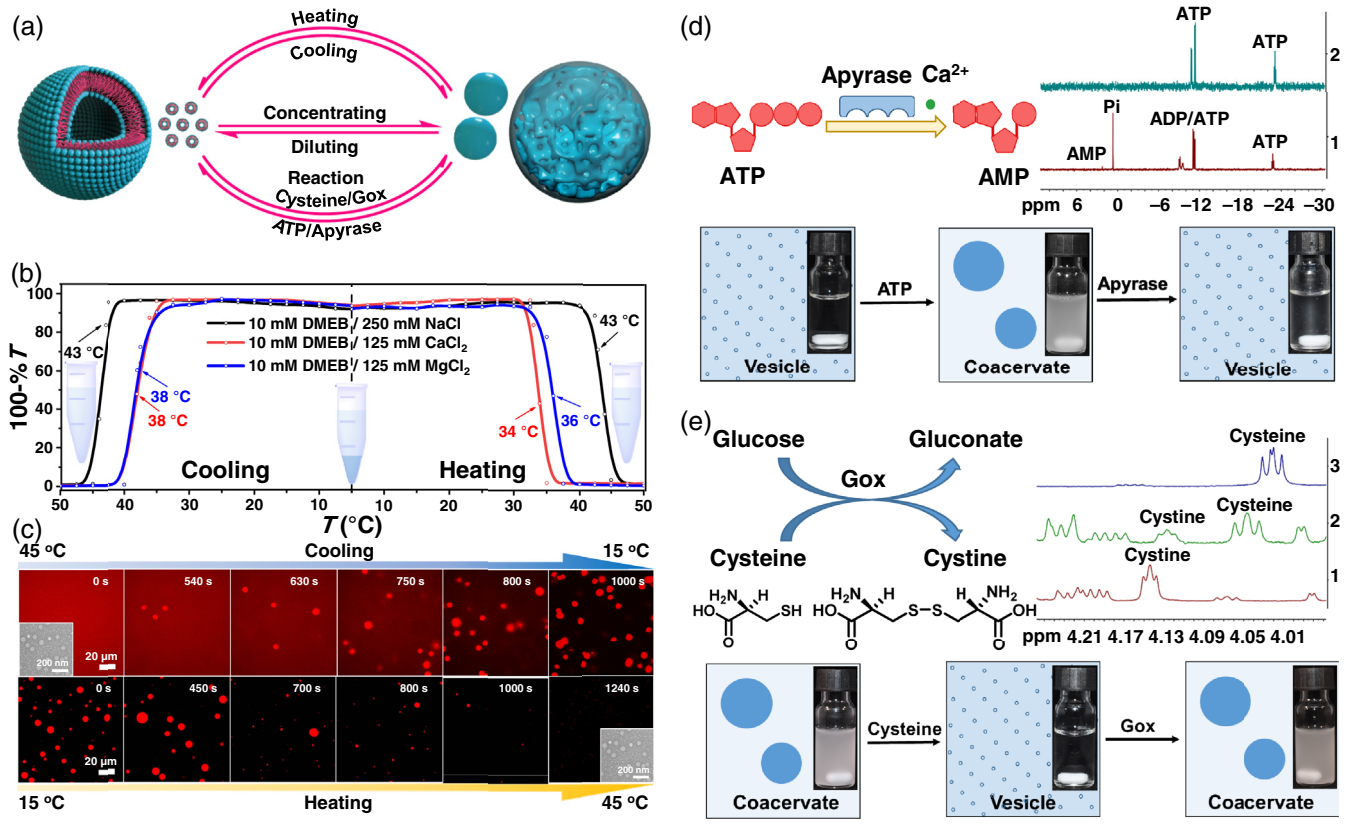

Figure 4 | *Phase transitions between vesicles and coacervates triggered by concentration, temperature, and enzymatic reactions. (a) Schematic representation of phase transitions in three approaches, including diluting or concentrating, heating or cooling, and chemical reactions. (b) Turbidimetric curves of 10 mM DMEB/250 mM NaCl, 10 mM DMEB/125 mM $CaCl_2$, and 10 mM DMEB/125 mM $MgCl_2$ mixtures at different temperature with heating and cooling, which independently induce the formation of vesicles or coacervates. (c) Confocal fluorescence images of the vesicle-to-coacervate and coacervate-to-vesicle transitions over time for 10 mM DMEB/140 mM NaCl solution with 20 μM rhodamine 6G by cooling and heating between 15 and 45 °C, respectively. The inset is a cryo-TEM image of vesicles in 10 mM DMEB/140 mM NaCl solution at 45 °C. Scale bar = 20 μm for all images. (d) Schematic representation of the ATP hydrolysis reaction, ^{31}P NMR of 10 mM DMEB/5 mM $CaCl_2$/5 mM ATP coacervates before and after the hydrolysis reaction, and schematic illustration of phase transition induced by ATP hydrolysis and the appearance of samples for each phase. (e) Schematic representation of a cascade reaction, in which glucose is oxidized to gluconate catalyzed by Gox, accompanied by the reduction of cysteine into cystine; the ^{1}H NMR of 20 mM DMEB/85 mM NaCl coacervates during the cascade reaction; and schematic illustration of the phase transition induced by the cascade reaction and the appearance of samples for each phase.*

had rapid and highly reproducible responsiveness to temperature change, which yields a critical temperature (T_φ) of 43 °C for 10 mM DMEB/250 mM NaCl and slightly lower ones for the two divalent salts (Figure 4b). Due to the weak permeability of vesicular membranes, 20 μM rhodamine 6G dispersed homogeneously in the vesicular bulk solution, not in the vesicles. As the temperature decreased from 45 to 15 °C, the homogeneous fluorescence signal disappeared gradually accompanied by the subsequent formation of coacervate droplets(Figure 4c and Supporting Information Movie S2). Upon increasing the temperature to 45 °C, the large red dots again became smaller and fewer, and the dots of about a few hundred nanometers were observed finally (Supporting Information Movie S3 and Figure S13). This might indicate that rhodamine 6G was encapsulated into the vesicles through this coacervate-to-vesicle transition process. It reveals that all the three DMEB/salt coacervates responded to temperature changes rapidly and the phase transitions were fully reversible and highly reproducible. Concentration is another readily variable environmental parameter. The phase diagrams of DMEB/salt systems show that the droplets transformed into vesicles and back into coacervates through diluting or concentrating. For example, a transparent 10 mM DMEB/180 mM NaCl solution became turbid after evaporation at room

DOI: 10.31635/ccschem.021.202000702
CCS Chem. **2021**, *3*, 358–366

temperature for 3 min. Vesicles were not large enough to be observed by optical microscopy, but the droplets became visible at higher total concentration (Supporting Information Figures S14a and S14b and Movie S4). On the contrary, the dilution processes induced the coacervate-to-vesicle transition, during which first, hollows appeared inside the droplet and then, the droplet became gradually smaller (Supporting Information Figure S14c and Movie S5).

Moreover, the formation and disassembly of coacervate droplets were controlled in an active manner by chemical reactions. First, we tested whether the ATP hydrolysis discussed above induced the transformation by converting a highly charged ATP into the weaker charged AMP (Figure 4d). Upon addition of 20 μL of 250 mM ATP solution, a 1 mL, 10 mM DMEB/5 mM $CaCl_2$ vesicular solution (Supporting Information Figure S15a) rapidly transformed into coacervates within a few seconds. Subsequently, 45 μL potato apyrase stock solution of 100 U/mL was added and the coacervate phase dissolved again along with the apyrase-catalyzed ATP hydrolysis into AMP, also confirmed by ^{31}P NMR (Figure 4d and Supporting Information S16). The highly charged ATP assisted the formation of coacervates due to the strong electrostatic interaction with oppositely charged DMEB and promoted the sequestration of enzymes, while product AMP with weaker charges had a destabilizing effect on coacervates by less electrostatic neutralization of DMEB headgroups. Next, we investigated whether the synthesis of complex molecules from simple ones could proceed in our coacervates and give rise to the opposite transformation, that is, coacervate → vesicle → coacervate. We designed a reaction pathway in which glucose oxidization to gluconate was catalyzed by Gox, accompanied by the reduction of cysteine into cystine triggered by the product in the last step (Figure 4e). Approximately, 20 μL of 250 mM cysteine solution resulted in the transition from coacervate phase to vesicular solution (20 mM DMEB/85 mM NaCl/0.1 mM NaI/5 mM glucose; Supporting Information Figure S15b). The negatively charged molecules predominantly localized in the headgroup region of DMEB, causing the packing parameter to become smaller and facilitating the formation of vesicles. Then 5 μL Gox solution of 4 mg/mL oxidized cysteine to cystine, resulting in the transformation of vesicles back into coacervates (Supporting Information Figure S17). The weakly water-soluble cystine was likely solubilized in the hydrophobic tail region of DMEB, causing it to swell and the curvature to become negative again. The coacervates that were formed provide a favorable environment for the weakly water-soluble cystine, coincidentally.

All above results confirmed that the surfactant-based coacervates were highly dynamic and capable of undergoing dynamic, reversible transition between a coacervate and vesicle, both of which can be viewed as an appearance state of this unique protocell. The transition was controlled by concentration, temperature, and chemical reactions, all of which could have been relevant mechanisms during the emergence of cell-like compartments from nonliving building blocks. Significantly, the coacervate-to-vesicle transition not only allowed for sequentially encapsulating solutes inside vesicles, but also demonstrated that small amphiphilic molecules can act as different functions during the evolution from protocell to modern cell.

Conclusion

We have developed a unique protocell capable of reversible transformation from a membrane-bound vesicle form to an open coacervate droplet form, based on a single-chain surfactant (DMEB) and monovalent or divalent inorganic salt in pure water. The coacervates can form at low DMEB concentration (>0.5 mM) and remain stable over a very broad range of salt concentration (up to saturation) and pH, facilitating adaptation to various environments and reaction conditions. Besides, a wide range of small molecular solutes (cationic, anionic, and hydrophobic dyes) and biomacromolecules (DNA and GFP) can be sequestrated within the coacervates at different pHs, attributed to the disordered sponge-like internal microstructure containing hydrophilic and hydrophobic domains. For the strong encapsulation ability of different species, the hydrolysis rate of ATP in coacervates has been enhanced compared with pure water, DMEB vesicles, and $CaCl_2$ aqueous solution, acting as an efficient bioreactor. Moreover, this reaction can drive the transition from coacervate to vesicle phase, whereas a cascade reaction to synthesize cystine from cysteine can induce the phase transition in the opposite direction. Adjusting concentration or temperature can also cause reversible and highly reproducible phase transition between vesicles and coacervates. These results demonstrate that simple surfactants can form coacervates only by the aid of inorganic salts. More importantly, the surfactant-based protocell model exhibits integrated features like polymer or polyelectrolyte systems, including easy formation, broad-spectrum sequestration, rate enhancement of enzymatic reactions, and coacervate-vesicle transition. Hence, this work represents a bottom-up approach to build protocell with simple components and could provide novel insights into the mechanisms of how surfactant-based protocells spatiotemporally control chemical reactions and coacervate–vesicle transitions.

Supporting Information

The Supporting Information is available and includes Experimental Methods, Supplementary Figures S1–S17,

DOI: 10.31635/ccschem.021.202000702
CCS Chem. **2021**, *3*, 358–366

Supplementary Table S1, Captions for Supplementary Movies S1–S5, and Movies S1–S5.

Conflict of Interest

There is no conflict of interest to report.

Acknowledgments

This work was supported by National Natural Science Foundation of China (grant nos. 21972149, 21988102, 21811530002, 21633002, and 21761142007).

References

1. Blain, J. C.; Szostak, J. W. Progress toward Synthetic Cells. *Annu. Rev. Biochem.* **2014**, *83*, 615–640.
2. Sakuma, Y.; Imai, M. From Vesicles to Protocells: The Roles of Amphiphilic Molecules. *Life* **2015**, *5*, 651–675.
3. Spoelstra, W. K.; Deshpande, S.; Dekker, C. Tailoring the Appearance: What Will Synthetic Cells Look Like? *Curr. Opin. Chem. Biol.* **2018**, *51*, 47–56.
4. Rideau, E.; Dimova, R.; Schwille, P.; Wurm, F. R.; Landfester, K. Liposomes and Polymersomes: A Comparative Review towards Cell Mimicking. *Chem. Soc. Rev.* **2018**, *47*, 8572–8610.
5. Aumiller, W. M., Jr.; Cakmak, F. P.; Davis, B. W.; Keating, C. D. RNA-Based Coacervates as a Model for Membraneless Organelles: Formation, Properties, and Interfacial Liposome Assembly. *Langmuir* **2016**, *32*, 10042–10053.
6. Douliez, J.-P.; Perro, A.; Béven, L. Stabilization of All-in-Water Emulsions to Form Capsules as Artificial Cells. *ChemBioChem* **2019**, *20*, 2546–2552.
7. Li, M.; Huang, X.; Tang, T.-Y. D.; Mann, S. Synthetic Cellularity Based on Non-Lipid Micro-Compartments and Protocell Models. *Curr. Opin. Chem. Biol.* **2014**, *22*, 1–11.
8. Deng, N.; Huck, W. T. S. Microfluidic Formation of Monodisperse Coacervate Organelles in Liposomes. *Angew. Chem. Int. Ed.* **2017**, *56*, 9736–9740.
9. Tang, T.-Y. D.; Hak, C. R. C.; Thompson, A. J.; Kuimova, M. K.; Williams, D. S.; Perriman, A. W.; Mann, S. Fatty Acid Membrane Assembly on Coacervate Microdroplets as a Step towards a Hybrid Protocell Model. *Nat. Chem.* **2014**, *6*, 527–533.
10. Vieregg, J. R.; Tang, T.-Y. D. Polynucleotides in Cellular Mimics: Coacervates and Lipid Vesicles. *Curr. Opin. Colloid Interface Sci.* **2016**, *26*, 50–57.
11. van Swaay, D.; Tang, T.-Y. D.; Mann, S.; de Mello, A. Microfluidic Formation of Membrane-Free Aqueous Coacervate Droplets in Water. *Angew. Chem. Int. Ed.* **2015**, *54*, 8398–8401.
12. Keating, C. D. Aqueous Phase Separation as a Possible Route to Compartmentalization of Biological Molecules. *Acc. Chem. Res.* **2012**, *45*, 2114–2124.
13. Alberti, S.; Gladfelter, A.; Mittag, T. Considerations and Challenges in Studying Liquid-Liquid Phase Separation and Biomolecular Condensates. *Cell* **2019**, *176*, 419–434.
14. Strulson, C. A.; Molden, R. C.; Keating, C. D.; Bevilacqua, P. C. RNA Catalysis through Compartmentalization. *Nat. Chem.* **2012**, *4*, 941–946.
15. Crosby, J.; Treadwell, T.; Hammerton, M.; Vasilakis, K.; Crump, M. P.; Williams, D. S.; Mann, S. Stabilization and Enhanced Reactivity of Actinorhodin Polyketide Synthase Minimal Complex in Polymer-Nucleotide Coacervate Droplets. *Chem. Commun.* **2012**, *48*, 11832–11834.
16. Sokolova, E.; Spruijt, E.; Hansen, M. M.; Dubuc, K. E.; Groen, J.; Chokkalingam, V.; Piruska, A.; Heus, H. A.; Huck, W. T. S. Enhanced Transcription Rates in Membrane-Free Protocells Formed by Coacervation of Cell Lysate. *Proc. Natl. Acad. Sci. U. S. A.* **2013**, *110*, 11692–11697.
17. Drobot, B.; Iglesias-Artola, J. M.; Vay, K. L.; Mayr, V.; Kar, M.; Kreysing, M.; Mutschler, H.; Tang, T.-Y. D. Compartmentalised RNA Catalysis in Membrane-Free Coacervate Protocells. *Nat. Commun.* **2018**, *9*, 3643–3651.
18. Aumiller, W. M., Jr.; Keating, C. D. Experimental Models for Dynamic Compartmentalization of Biomolecules in Liquid Organelles: Reversible Formation and Partitioning in Aqueous Biphasic Systems. *Adv. Colloid Interface Sci.* **2017**, *239*, 75–87.
19. Poudyal, R. R.; Cakmak, F. P.; Keating, C. D.; Bevilacqua, P. C. Physical Principles and Extant Biology Reveal Roles for RNA-Containing Membraneless Compartments in Origins of Life Chemistry. *Biochemistry* **2018**, *57*, 2509–2519.
20. Zhuang, M.; Zhang, Y.; Zhou, S.; Zhang, Y.; Wang, K.; Nie, J.; Liu, J. Uricase-Containing Coacervate Microdroplets as Enzyme Active Membrane-Free Protocells for Detoxification of Uric Acid in Serum. *Chem. Commun.* **2019**, *55*, 13880–13883.
21. Deamer, D. W. Membrane Compartments in Prebiotic Evolution. In *The Molecular Origins of Life*;Brack, A., ed.; Cambridge University Press: Cambridge, U.K., **1998**; Vol. 8, pp 189–205.
22. Dzieciol, A. J.; Mann, S. Designs for Life: Protocell Models in the Laboratory. *Chem. Soc. Rev.* **2012**, *41*, 79–85;
23. Ruiz-Mirazo, K.; Briones, C.; de la Escosura, A. Prebiotic Systems Chemistry: New Perspectives for the Origins of Life. *Chem. Rev.* **2014**, *114*, 285–366.
24. Thomas, J. A.; Rana, F. R. The Influence of Environmental Conditions, Lipid Composition, and Phase Behavior on the Origin of Cell Membranes. *Orig. Life Evol. Biosph.* **2007**, *37*, 267–285.
25. Garenne, D.; Beven, L.; Navailles, L.; Nallet, F.; Dufourc, E. J.; Douliez, J.-P. Sequestration of Proteins by Fatty Acid Coacervates for Their Encapsulation within Vesicles. *Angew. Chem. Int. Ed.* **2016**, *55*, 13475–13479.
26. Douliez, J.-P.; Martin, N.; Gaillard, C.; Beneyton, T.; Baret, J.-C.; Mann, S.; Beven, L. Catanionic Coacervate Droplets as a Surfactant-Based Membrane-Free Protocell Model. *Angew. Chem. Int. Ed.* **2017**, *56*, 13689–13693.
27. Koga, S.; Williams, D. S.; Perriman, A. W.; Mann, S. Peptide–Nucleotide Microdroplets as a Step towards a Membrane-Free Protocell Model. *Nat. Chem.* **2011**, *3*, 720–724.
28. Wang, M.; Wang, Y. L. Development of Surfactant Coacervation in Aqueous Solution. *Soft Matter* **2014**, *10*, 7909–7919.

29. Zhao, W.; Wang, Y. L. Coacervation with Surfactants: From Single-Chain Surfactants to Gemini Surfactants. *Adv. Colloid Interface Sci.* **2017**, *239*, 199–212.
30. Aumiller, W. M., Jr.; Keating, C. D. Phosphorylation-Mediated RNA/Peptide Complex Coacervation as a Model for Intracellular Liquid Organelles. *Nat. Chem.* **2016**, *8*, 129–137.
31. Nakashima, K. K.; Baaij, J. F.; Spruijt, E. Reversible Generation of Coacervate Droplets in an Enzymatic Network. *Soft Matter* **2018**, *14*, 361–367.
32. Martin, N.; Tian, L.; Spencer, D.; Coutable-Penarun, A.; Ross Anderson, J. L.; Mann, S. Photoswitchable Phase Separation and Oligonucleotide Trafficking in DNA Coacervate Microdroplets. *Angew. Chem. Int. Ed.* **2019**, *58*, 14594–14598.
33. Ianiro, A.; Wu, H.; van Rijt, M. M. J.; Vena, M. P.; Keizer, A. D. A.; Esteves, A. C. C.; Tuinier, R.; Friedrich, H.; Sommerdijk, N. A. J. M.; Patterson, J. P. Liquid–Liquid Phase Separation During Amphiphilic Self-Assembly. *Nat. Chem.* **2019**, *11*, 320–328.
34. Martin, N. Dynamic Synthetic Cells Based on Liquid–Liquid Phase Separation. *ChemBioChem* **2019**, *20*, 2553–2568;
35. Jang, Y.; Hsieh, M.-C.; Dautel, D.; Guo, S.; Grover, M. A.; Champion, J. A. Understanding the Coacervate-to-Vesicle Transition of Globular Fusion Proteins to Engineer Protein Vesicle Size and Membrane Heterogeneity. *Biomacromolecules* **2019**, *20*, 3494–3503.
36. Martin, N.; Douliez, J.-P.; Qiao, Y.; Booth, R.; Li, M.; Mann, S. Antagonistic Chemical Coupling in Self-Reconfigurable Host–Guest Protocells. *Nat. Commun.* **2018**, *9*, 3652–3613.
37. Roy, S.; Khatua, D.; Dey, J. Giant Vesicles of a Single-Tailed Chiral Cationic Surfactant, (1*R*,2*S*)-(−)-*N*-Dodecyl-*N*-Methylephedrinium Bromide, in Water. *J. Colloid Interface Sci.* **2005**, *292*, 255–264.
38. Páhi, A. B.; Varga, D.; Király, Z.; Mastalir, A. Thermodynamics of Micelle Formation of the Ephedrine-Based Chiral Cationic Surfactant DMEB in Water, and the Intercalation of DMEB in Montmorillonite. *Colloids Surf. A* **2008**, *319*, 77–83.
39. Deamer, D. W. The Role of Lipid Membranes in Life's Origin. *Life* **2017**, *7*, 5.
40. Valenzuela, M. A.; Kettlun, A. M.; Mancilla, M.; Calvo, V.; Fanta, N.; Traverso-Cori, A. The Effect of Bivalent Metal Ions on ATPase-ADPase Activities of Apyrase from *Solanum tuberosum*. *Phytochemistry* **1988**, *27*, 1981–1985.
41. Maiti, S.; Fortunati, I.; Ferrante, C.; Scrimin, P.; Prins, L. J. Dissipative Self-Assembly of Vesicular Nanoreactors. *Nat. Chem.* **2016**, *8*, 725–732.
42. Li, L.; Prywes, N.; Tam, C. P.; O'Flaherty, D. K.; Lelyveld, V. S.; Izgu, E. C.; Pal, A.; Szostak, J. W. Enhanced Nonenzymatic RNA Copying with 2-Aminoimidazole Activated Nucleotides. *J. Am. Chem. Soc.* **2017**, *139*, 1810–1813.
43. O'Flaherty, D. K.; Zhou, L.; Szostak, J. W. Nonenzymatic Template-Directed Synthesis of Mixed-Sequence 3′-NP-DNA up to 25 Nucleotides Long Inside Model Protocells. *J. Am. Chem. Soc.* **2019**, *141*, 10481–10488.
44. Menger, F. M.; Seredyuk, V. A.; Apkarian, R. P.; Wright, E. R. Colloidal Assemblies of Branched Geminis Studied by Cryo-Etch-HRSEM. *J. Am. Chem. Soc.* **2002**, *124*, 12408–12409.
45. Novak, S.; Piperčić, S. M.; Makarić, S.; Primožič, I.; Ćurlin, M.; Štefanić, Z.; Jurasin, D. D. Interplay of Noncovalent Interactions in Ionic Liquid/Sodium Bis(2-ethylhexyl) Sulfosuccinate Mixtures: From Lamellar to Bicontinuous Cubic Liquid Crystalline Phase. *J. Phys. Chem. B* **2016**, *120*, 12557–12567.
46. Bracha, D.; Walls, M. T.; Brangwynne, C. P. Probing and Engineering Liquid-Phase Organelles. *Nat. Biotechnol.* **2019**, *37*, 1435–1445.
47. Nakashima, K. K.; Vibhute, M. A.; Spruijt, E. Biomolecular Chemistry in Liquid Phase Separated Compartments. *Front. Mol. Biosci.* **2019**, *6*, 21.
48. Garenne, D.; Navailles, L.; Nallet, F.; Grélard, A.; Dufourc, E. J.; Douliez, J.-P. Clouding in Fatty Acid Dispersions for Charge-Dependent Dye Extraction. *J. Colloid Interface Sci.* **2016**, *468*, 95–102.
49. Serrano-Luginbühl, S.; Ruiz-Mirazo, K.; Ostaszewski, R.; Gallou, F.; Walde, P. Soft and Dispersed Interface-Rich Aqueous Systems that Promote and Guide Chemical Reactions. *Nat. Rev. Chem.* **2018**, *2*, 306–327.
50. Elani, Y.; Law, R. V.; Ces, O. Vesicle-Based Artificial Cells as Chemical Microreactors with Spatially Segregated Reaction Pathways. *Nat. Commun.* **2014**, *5*, 5305–5310.
51. Paudel, B. P.; Rueda, D. Molecular Crowding Accelerates Ribozyme Docking and Catalysis. *J. Am. Chem. Soc.* **2014**, *136*, 16700–16703.
52. Yamagami, R.; Bingaman, J. L.; Frankel, E. A.; Bevilacqua, P. C. Cellular Conditions of Weakly Chelated Magnesium Ions Strongly Promote RNA Stability and Catalysis. *Nat. Commun.* **2018**, *9*, 2149–2160.